ARTICLES
PUBLISHED ONLINE: 14 MARCH 2016 | DOI: 10.1038/NGEO2674
nature geoscience

Pan-Arctic ice-wedge degradation in warming permafrost and its influence on tundra hydrology

Anna K. Liljedahl[1]*, Julia Boike[2], Ronald P. Daanen[3], Alexander N. Fedorov[4], Gerald V. Frost[5], Guido Grosse[6], Larry D. Hinzman[7], Yoshihiro Iijma[8], Janet C. Jorgenson[9], Nadya Matveyeva[10], Marius Necsoiu[11], Martha K. Raynolds[12], Vladimir E. Romanovsky[13,14], Jörg Schulla[15], Ken D. Tape[1], Donald A. Walker[12], Cathy J. Wilson[16], Hironori Yabuki[17] and Donatella Zona[18,19]

Ice wedges are common features of the subsurface in permafrost regions. They develop by repeated frost cracking and ice vein growth over hundreds to thousands of years. Ice-wedge formation causes the archetypal polygonal patterns seen in tundra across the Arctic landscape. Here we use field and remote sensing observations to document polygon succession due to ice-wedge degradation and trough development in ten Arctic localities over sub-decadal timescales. Initial thaw drains polygon centres and forms disconnected troughs that hold isolated ponds. Continued ice-wedge melting leads to increased trough connectivity and an overall draining of the landscape. We find that melting at the tops of ice wedges over recent decades and subsequent decimetre-scale ground subsidence is a widespread Arctic phenomenon. Although permafrost temperatures have been increasing gradually, we find that ice-wedge degradation is occurring on sub-decadal timescales. Our hydrological model simulations show that advanced ice-wedge degradation can significantly alter the water balance of lowland tundra by reducing inundation and increasing runoff, in particular due to changes in snow distribution as troughs form. We predict that ice-wedge degradation and the hydrological changes associated with the resulting differential ground subsidence will expand and amplify in rapidly warming permafrost regions.

Up to two-thirds of the Arctic landscape is occupied by wetlands and non-mountain areas[1] that store large amounts of carbon in the climate-sensitive near-surface permafrost soils[2,3]. During the past few decades, larger thermokarst lakes have increased in number and area[4,5], whereas smaller water bodies (~100 m^2) in vegetated drained thaw lake basins decreased[6]—all at a time when field measurements and climate reanalyses indicate an intensification of the pan-Arctic water cycle, notably increased runoff[7] and modelled evapotranspiration[8]. Multiple mechanisms have been suggested to explain this intensification, including enhanced poleward atmospheric moisture transport[9], permafrost thaw[4] along with increased active layer depths and baseflow[10], and higher evapotranspiration due to lengthening of the thaw season[11]. The early observations of altered tundra microtopography due to melting of ice wedges and differential ground subsidence[12] have yet to enter the discussion as a mechanism behind the pan-Arctic intensification of the water cycle. Model experiments, which excluded the representation of frozen ground, introduced the importance of ice-wedge polygon type on watershed-scale hydrology, including evapotranspiration, water levels and runoff[13].

Ice wedges form over timescales of centuries to millennia, whereas melting of its uppermost portion can occur within decades. During formation, snowmelt water infiltrates into thermal contraction cracks that are several metres deep, which develop during winter cold spells[14,15]. Repeating the process for many years forms a wedge-shaped ice body that may be several metres in width at the top, and which upturns overlying and adjacent soil strata by plastic deformation. The elevated ridges result in polygonal relief development, which constitutes the rampart of 5–30 m-diameter low-centred polygons (LCPs; ref. 16). High-centred polygons (HCPs) exhibit the inverse topography of LCPs, where well-drained mounds are surrounded by troughs above

[1]Water and Environmental Research Center, University of Alaska Fairbanks, 306 Tanana Loop, Fairbanks, Alaska 99775, USA. [2]Alfred Wegener Institute Helmholtz Centre for Polar and Marine Research, Telegrafenberg A6, 14473 Potsdam, Germany. [3]Department of Natural Resources, Division of Geological and Geophysical Surveys, 3354 College Road, Fairbanks, Alaska 99709, USA. [4]Melnikov Permafrost Institute, 36 Merzlotnaya Street, 677010 Yakutsk, Russia. [5]ABR, Inc. Environmental Research and Services, PO Box 80410, Fairbanks, Alaska 99709, USA. [6]Alfred Wegener Institute Helmholtz Centre for Polar and Marine Research, Telegrafenberg A45, 14473 Potsdam, Germany. [7]International Arctic Research Center, University of Alaska Fairbanks, 930 Koyukuk Drive, Fairbanks, Alaska 99775, USA. [8]Institute of Arctic Climate and Environmental Research, Japan Agency for Marine-Earth Science and Technology, 2-15 Natsushima-machi, Yokosuka-city, Kanagawa 237-0061, Japan. [9]Arctic National Wildlife Refuge, 101 12th Avenue, Fairbanks, Alaska 99701, USA. [10]Komarov Botanical Institute, Russian Academy of Sciences, Popova Street 2, St Petersburg 197376, Russia. [11]Southwest Research Institute, Geosciences and Engineering Division, 6220 Culebra Road, San Antonio, Texas 78238, USA. [12]Institute of Arctic Biology, University of Alaska Fairbanks, 902 North Koyukuk Drive, PO Box 757000, Fairbanks, Alaska 99775, USA. [13]Geophysical Institute, University of Alaska Fairbanks, 903 Koyukuk Drive, Fairbanks, Alaska 99775, USA. [14]Earth Cryosphere Institute, 86 Malygina Street, Tyumen 625000, Russia. [15]Hydrology Software Consulting, Regensdorferstrasse 162, CH-8049 Zurich, Switzerland. [16]Earth and Environmental Sciences Division, Los Alamos National Laboratory, MS J495, Los Alamos, New Mexico 87545, USA. [17]Department of Environmental Geochemical Cycle Research, Japan Agency for Marine-Earth Science and Technology, 3173-25 Showa-machi, Kanazawa-ku, Yokohama-city, Kanagawa 236-0001, Japan. [18]Department of Biology, San Diego State University, San Diego, California 92182, USA. [19]Department of Animal and Plant Sciences, University of Sheffield, Sheffield S10 2TN, UK.
*e-mail: akliljedahl@alaska.edu

© 2016 Macmillan Publishers Limited. All rights reserved

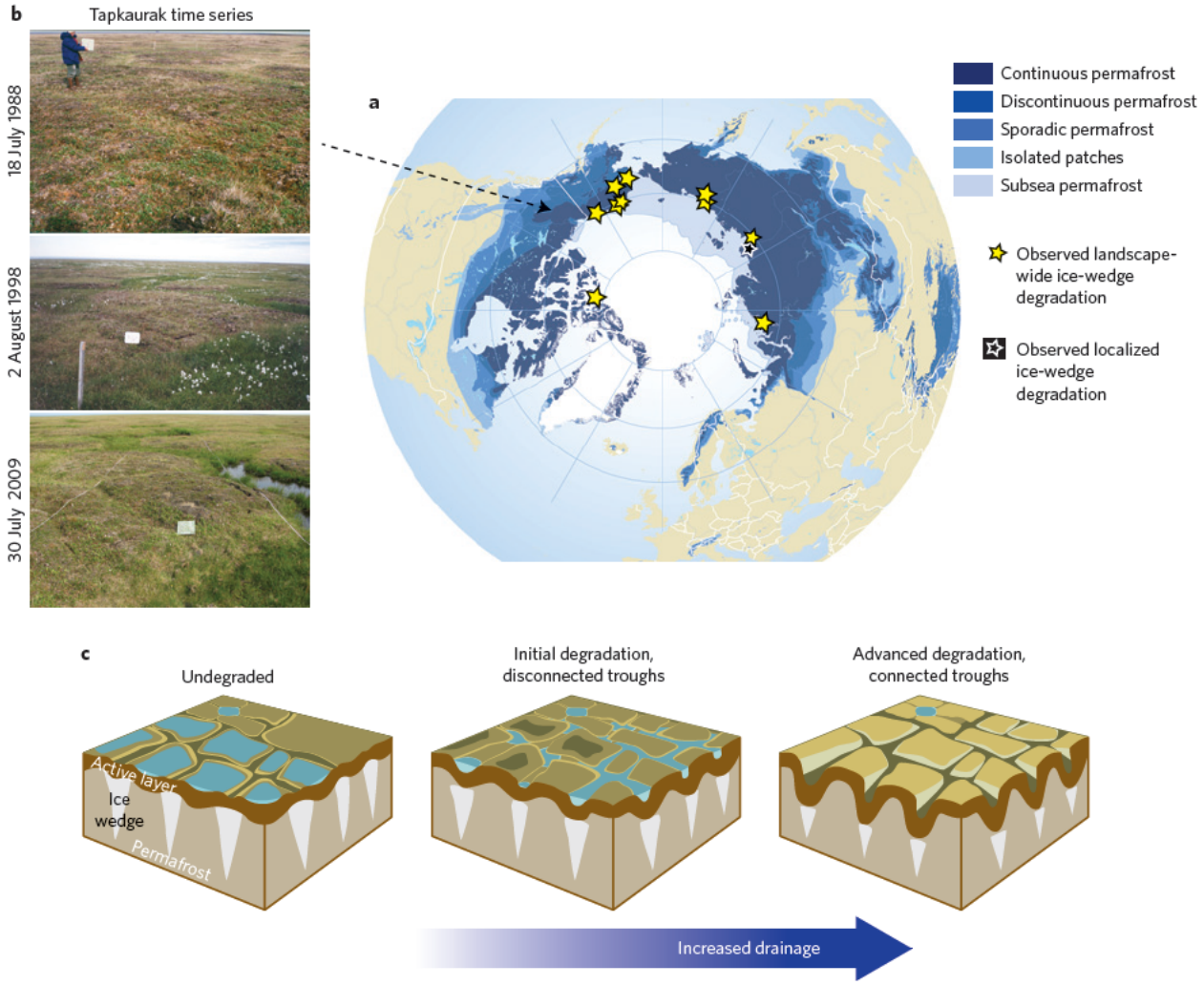

Figure 1 | Observed recent ice-wedge degradation and a schematic of its hydrological impacts. a,b, Sites with observed ice-wedge degradation in the continuous permafrost region[42] (**a**), which led to changes in surface water and vegetation as seen at Tapkaurak, Alaska (**b**). **c**, Schematic representation of the polygon succession, including the undegraded stage with inundated low-centred polygon centres or non-patterned ground, the initial degradation stage with disconnected troughs, where the tops of the ice wedges have melted forming trough-ponds that surround low- or high-centred polygons, and the advanced degradation stage with connected troughs, which represents a laterally connected, well-drained trough-network, mounds and high-centred polygons.

degraded ice wedges. At the landscape scale, wedge ice is estimated to represent ~20% or more of the uppermost permafrost volume, highlighting the enormous potential for differential thaw subsidence[17–20]. The permafrost warming that started two to three decades ago has been especially rapid in cold-continuous permafrost[21]. Simulations suggest that warming mean annual air temperatures of +5 °C can initiate subsidence after 15–50 years at the Canadian High Arctic[22]. Landscape-averaged subsidence due to ground ice loss has been measured by means of field-based surveys[23] and high-resolution remote sensing methods in Northern Alaska and Russia[24,25]. The differential ground subsidence has transformed LCPs or non-patterned ground into HCPs within a few decades in Alaska[12,20,26–28] and Canada[29].

Stark physical and biological variability at the sub-metre scale are typical of ice-wedge polygon landscapes. Differences in near-surface soil moisture[30], plant distribution[31], snow accumulation[32], soil biological activity[33] and carbon flux[34,35] are linked to polygon features. Centres of LCPs are often inundated during summer[36–38], whereas mounds of HCPs are well-drained and their troughs may serve as effective snow traps and hydrologic pathways during snowmelt[39]. The direction and magnitude of carbon, water and energy feedback to climate, including permafrost aggradation or degradation, is strongly controlled by the unique biogeophysical characteristics within the respective ice-wedge polygon features[20,28,35].

Observations of ice-wedge degradation

On-site observations combined with high-resolution remote sensing imagery show widespread ice-wedge degradation in several Arctic sites during recent decades (Fig. 1a). Landscape-wide ice-wedge degradation was observed at ten out of our eleven sites. Our field efforts identified recent ice-wedge degradation through a range of markers: a mismatch between vegetation type and soil moisture regime, changes in vegetation composition, top-of-permafrost temperatures crossing the 0 °C threshold, as well as ponding or drying and ground subsidence by nearly one metre.

The vegetation at the Tapkaurak site, Arctic Alaska, is characteristic of many areas that have undergone ice-wedge degradation. Changes in vegetation were the first signs of degradation, which resulted in an overall decreased moss (40–16%) and lichen cover (30–8%) from 1986 to 2009 and, above ice wedges, an increase in water-tolerant sedges (2–11%)

© 2016 Macmillan Publishers Limited. All rights reserved

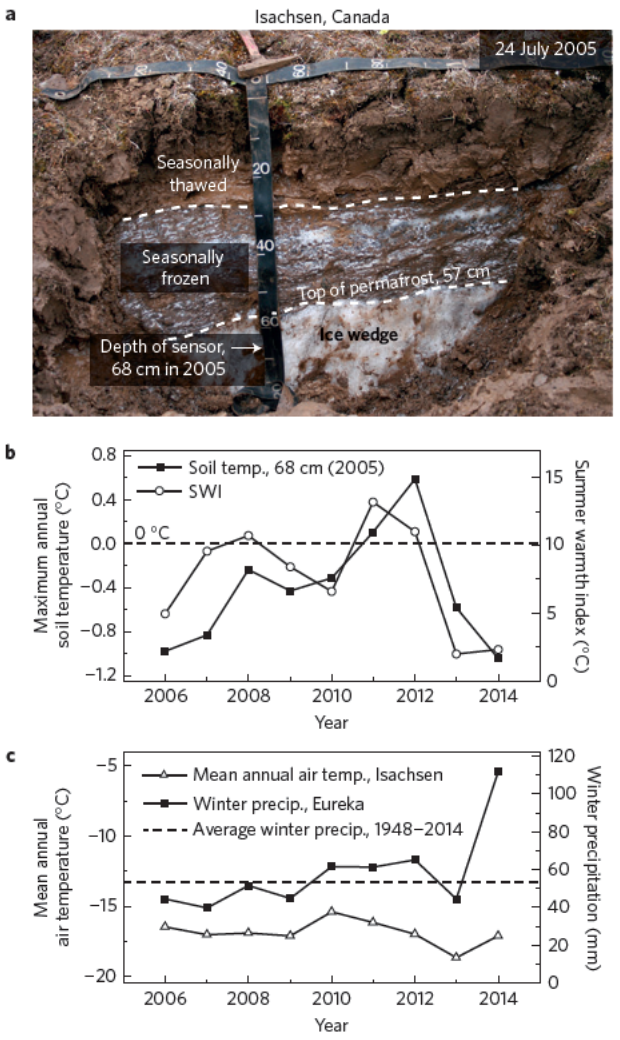

Figure 2 | Thawing permafrost and ice-wedge tops, Isachsen, Canadian High Arctic. a, Partially thawed active layer in contact with the top of the ice wedge in 2005. A soil temperature sensor was installed at 68 cm depth in 2005. Subsidence and frost heave changed the sensor depth to 44 cm by 2013. **b**,**c**, Soil temperatures rose above 0 °C in 2011 and 2012 (**b**) and ground subsidence (Supplementary Fig. 3) shows ice-wedge melting. The above freezing soil temperatures coincide with a high Summer Warmth Index (SWI) (**b**), which is the sum of mean monthly air temperature above 0 °C, and slightly above average winter precipitation (**c**).

(Fig. 1b and Supplementary Fig. 1)[26]. In addition, new wetland species were found in the more recent years, including the aquatic grass *Dupontia fisheri*, which did not previously grow at the Tapkaurak site. Also, as the degradation progressed, small trough-ponds evolved, resulting in a water coverage increase from 0 to 22% across the surveyed vegetation transect. This type of species composition change is indicative of a lasting morphological and hydrological change, and not due to seasonal anomalies in moisture (for example, rainfall).

The previously smooth, non-patterned landscape at Tareya, High Arctic Siberia, became polygonized with a network of troughs that were 2–3 m wide and 0.3–0.9 m deep, with its surrounding flat-top mounds reaching 7–10 m in diameter (Supplementary Fig. 2). A general greening in troughs was observed, but only limited changes in plant species composition, structure or distribution. A few vascular plant species that were rare in the past (1970) were not found in 2010, whereas the abundance of *Hierochloe pauciflora* and *Carex chordorrhiza* decreased and *C. stans* increased[40]. Other sites at Tareya, which previously exhibited sharp contrast in plant species between low centres and raised rims (1.5–2 m wide and 0.3–0.4 m high), became a non-patterned landscape after the old rim surfaces sank to the level of the polygon centre. Consequently, the remnant mesic plant communities on polygon rims were last observed in an identical moisture regime as the hydric mire herbs and mosses.

At the lichen-moss hummock area at Isachsen, High Arctic Canada, the previously even ground surface showed ~0.5 m deep troughs after a return to the site eight years later (Fig. 2 and Supplementary Fig. 3). Ice content of the seasonally frozen portion of the active layer ranged from 40 to 60% during site installation in late July 2005, where the top of permafrost was represented by an ice wedge. Soil temperature measurements located 11 cm into the permafrost (in 2005) confirm permafrost degradation as the warmest temperatures exceeded 0 °C (2011 and 2012), with maximum annual temperatures later returning to below freezing (Fig. 2b). Further, the distance between the ground surface and the sensor decreased from 68 cm (2005) to 44 cm (2013) owing to thawing of ice-rich permafrost and some frost heave.

At Prudhoe Bay, Arctic Alaska, the trough development resulted in wetter plant communities in the new depressions, with more well-drained plant communities in the polygon centres. Ponds that were initially confined to small areas at the intersections of ice wedges expanded along the length of polygon troughs, and many became linked to each other (Supplementary Fig. 4). A ground survey of near-surface soil moisture highlights the wet, nearly saturated conditions in the bottom of a depression, which was formed by top-melting of ice wedges, and the gradual near-surface drying up towards the surrounding mounds. A repeat of the survey nine years later shows that the trough has widened, with the centre now slightly elevated (most likely owing to sediment infilling from the eroding sides). A widening of the depressions was also observed at Tiksi, Russia, which included a lateral expansion of troughs (Supplementary Fig. 5). At the Kolyma site, at the forest–tundra ecotone in northeast Siberia, ice-wedge degradation led to a substantial mortality of larch, which previously grew on raised and relatively well-drained microsites associated with rims of wide LCPs (ref. 41). The marked microtopographical inversion resulted in extensive trough-pond formation where larch trees once stood (Supplementary Fig. 6a). Together, our field observations at widespread sites across the Arctic domain recognize ice-wedge degradation via an assortment of ecological states, from relatively subtle mismatches between vegetation type and soil moisture, transitioning into the more marked appearance of flooded pits.

Detection of ice-wedge degradation using high-resolution satellite imagery primarily included alterations to surface wetness and the appearance or disappearance of small (~5 to ~50 m^2) ponds (Fig. 3 and Supplementary Figs 4, 6 and 7). Typically, polygon centres that were previously inundated developed a reduced surface wetness, whereas ground above ice wedges experienced wetting. No wetting polygon centres were observed. Ponds that were initially confined to the intersections of ice wedges expanded along the length of polygon troughs and became increasingly interconnected (Supplementary Fig. 6b). Our observations also included sites with drying troughs, oftentimes when nearby trough systems experienced simultaneous wetting (Fig. 3b). Drying above ice wedges was especially prevalent at Chukochy, Russia, where trough-ponds were widespread in the upland tundra landscape in 1965, but had largely disappeared by 2009 (Fig. 3c).

Polygon succession and hydrologic transition

Our observations suggest a general morphological evolution, a polygon succession, in low-gradient tundra hydrology that include two major hydrological states, which are separated by the absence/presence of lateral surface water connectivity (Fig. 1c). The initial degradation stage with disconnected troughs is primarily

© 2016 Macmillan Publishers Limited. All rights reserved

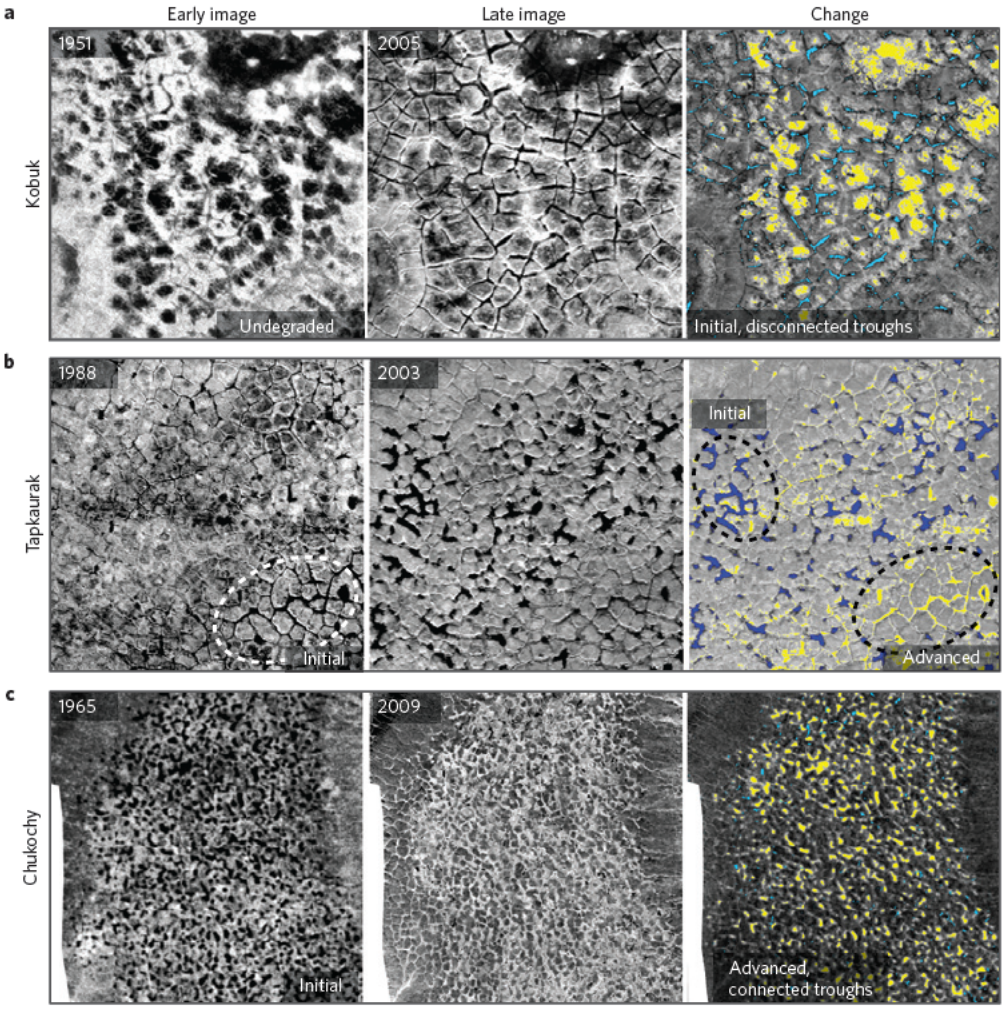

Figure 3 | Observed ice-wedge degradation using aerial photos, satellite imagery and change-detection analysis. a–c, Time series of three landscapes showing polygon succession from the undegraded stage (**a**: Kobuk 1951) to the initial stage with disconnected trough-ponds (**a**: Kobuk 2005, **c**: Chukochy 1965, **b**: Tapkaurak 1988 and 2003) and the advanced stage with drained connected troughs (**b**: Tapkaurak 2003 and **c**: Chukochy 2009). An increase in surface moisture (blue) is seen above the ice-wedge network at the initial stage (**a**,**b**), whereas the advanced stage (**c**) show reduced moisture (yellow). Low-centred polygon centres show drying when transitioning from the undegraded to the initial degradation stage. Domains are 250 × 250 m (Kobuk, Tapkaurak) and 500 × 500 m (Chukochy).

characterized by the formation of new troughs and isolated surface water above ice wedges, accompanied, if melting of wedge ice occurs in LCP tundra, by draining of polygon centres (Fig. 3a,b). Here, landscapes of previously low geographical wetness variability become increasingly heterogeneous (polygon centres dry and trough-ponds form). Early indicators of the initial degradation stage include subtle changes in vegetation, which, as the top wedge ice continues to melt, may evolve into trough-ponds. Continued ice-wedge melting leads to the advanced degradation stage with connected troughs, which promotes the lateral expansion of individual ponds via a network of troughs. The trough-network expansion across a hydraulic gradient may ultimately result in drainage across the entire (Fig. 3c) or portions of the landscape (Fig. 3b). At the Isachsen site, the 2% slope probably allowed the newly formed troughs to drain immediately (Supplementary Fig. 3). At the Chukochy site, the trough-network most likely expanded across a hydraulic gradient from yedoma uplands into surrounding thermokarst basins that drained the trough-ponds (Fig. 3c). The ice wedges at Chukochy are wide (5–10 m) and surrounding permafrost is ice-rich (50–90%; ref. 41), preventing sediment infilling of troughs (slumping sides) that otherwise can promote permafrost aggradation[20].

Rapid changes at sub-decadal timescales

Locations where on-site or imagery observations are most frequent highlight the rapid progression of ice-wedge degradation. Preceded by a relatively stable landscape from 1949 through to the mid-1980s (ref. 28), the majority of flooded troughs appeared within an 11-year time period (1990–2001) at Prudhoe Bay, which was followed by an expansion of the trough-ponds (2001–2010) (Supplementary Fig. 4). A widening and lateral expansion of existing troughs was also observed within a recent ten-year period at Tiksi, Russia (Supplementary Fig. 5). Tareya, Russia, was visited every decade since the mid 1960s for long-term botanical studies. The non-patterned landscape showed no signs of ice-wedge polygons up through the 1994 field effort, but a well-developed trough system was evident in high-resolution imagery by 2003 (Supplementary Fig. 2). The 1994–2003 ice-wedge degradation was confirmed during a 2010 field visit. At Isachsen, Canada, several vegetation study plots established on a non-patterned surface in 2005 had transformed by August 2013 into mounds surrounded by troughs (Supplementary Fig. 3). Soil temperatures constrain the subsidence event, as defined as the thaw of at least the upper 11 cm of the permafrost, to summer 2011 and 2012 (Fig. 2). At Tapkaurak, Alaska, subtle changes in the vegetation

© 2016 Macmillan Publishers Limited. All rights reserved

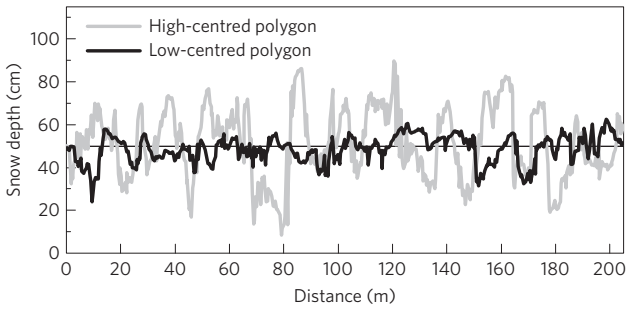

Figure 4 | Measured snow distribution across polygons representing undegraded and advanced degradation stages, Barrow, Alaska. The presence of well-developed troughs at the advanced degradation stage (high-centred polygons, HCPs) increased the variability in snow depth. However, the average (horizontal line) end-of-winter snow depth at HCPs was statistically similar to that of the undegraded stage (low-centred polygons, LCPs) (50 ± 15 and 50 ± 7 cm, respectively, *t*-test, 0.05 level, equal variance not assumed).

above the ice wedges were observed between the 1988 and 1991 field visits (Figs 1b and 3b and Supplementary Fig. 1). By 1998, clearly visible troughs had formed and were reflected in the vegetation patterns. Small trough-ponds had formed after another four years (2002), which were also identified in 2003 high-resolution imagery, and had further widened by 2009. In summary, the initial degradation stage with disconnected troughs was initiated within a 9- to 11-year time period (Prudhoe Bay, Tareya, and Tapkaurak) and sustained for several decades (Kolyma, Kobuk, Barrow, Seward Peninsula). The transition to the advanced stage with connected troughs ranged from 15 years (Tapkaurak) to within four decades (Chukochy), whereas the newly formed troughs at the slopes of the Isachsen site presented a well-drained connected trough-network within 8 years. The observed trough formation at otherwise undisturbed cold-continuous permafrost landscapes is evidently a phenomenon taking place at often recent, sub-decadal periods, although antecedent development (expansion of troughs, drying or wetting across the landscape), as can been seen from early ground subsidence (pre-1980), may continue for several decades.

Hydrologic implications

A space-for-time substitution can provide insights into the impact of ice-wedge degradation on hydrology. Landscapes dominated by low- (LCP) or high-centred polygons (HCPs) present statistically similar averaged end-of-winter snow accumulation. In Barrow, Alaska, landscape-averaged snow depth was 50 cm in early May, whereas the spatial variability was nearly double at the HCPs compared to the LCPs in 2012 (s.d. ± 15 and 7 cm, respectively, Fig. 4). Snowmelt produced >20 cm deep inundation at both the troughs and the LCP centres (Fig. 5). The LCPs experienced the least variability in seasonal and interannual water table, with a continuous inundation in 2013 and 2014. Both June 2014 and mid-summer 2014 had record high rainfall. In 2012, which experienced below normal early through mid-summer rainfall, the LCP centre water table was, at most, 5 cm below the ground surface. Centres of HCPs saw no snowmelt inundation, but rather a rapid rise and fall in water table in conjunction with larger precipitation events. The surface water coverage of the trough was discontinuous in 2012, with a nearly 20 cm drawdown during the abnormally low rainfall in early summer. Throughout this interannual variability, centres of LCPs and HCPs represented the hydrological extremes of nearly continuous wetness (LCP) or dryness (HCP), whereas the inundation of the trough was concentrated to snowmelt and during periods with typical or above-average summer precipitation.

Numerical model experiments informed by field measurements and LiDAR-derived topography (0.25-m spatial resolution) can help

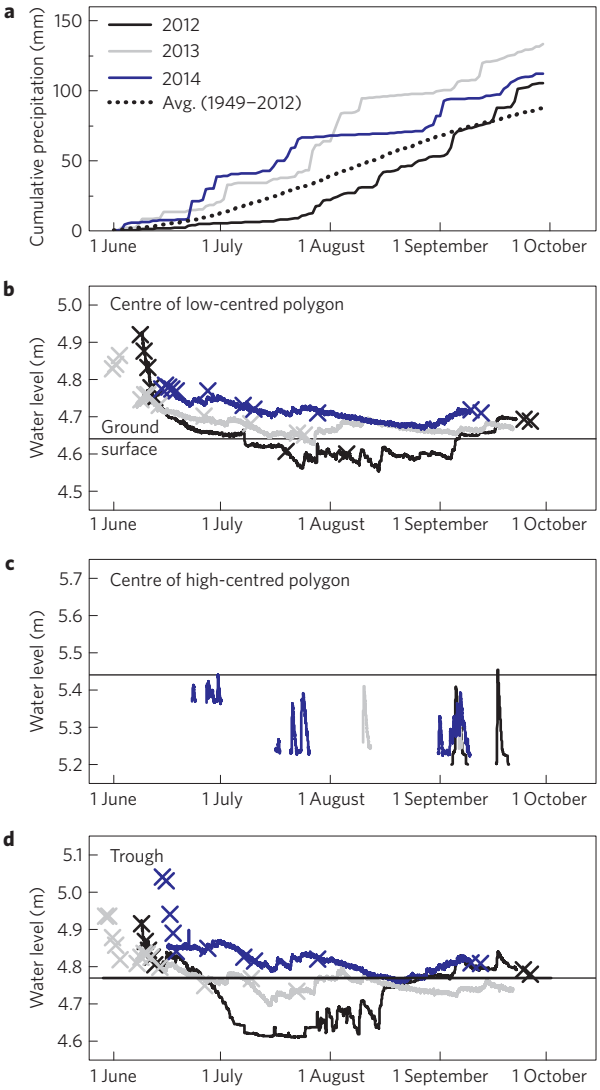

Figure 5 | Measured water levels in different ice-wedge polygon types, Barrow, Alaska. a, Cumulative summer precipitation (1 June–1 October) in 2012–2014 and the long-term average (1949–2012), where 2012 received below-average precipitation in early summer and 2013 and 2014 received above-average precipitation. **b**–**d**, Water levels measured manually (crosses) and with instrumentation (lines) show inundation following snowmelt in well-developed troughs (**d**) and LCP centres (**b**), in which water tables remain near the surface. The HCP mounds (**c**) show flashy responses to individual events. Site photos during snowmelt inundation are presented in the Supplementary Information (Supplementary Fig. 9).

us distil the known metre-scale complexity to assess the impacts of ice-wedge degradation on watershed-scale hydrology. Among the modelled scenarios, it was only the LCP-dominated watershed that exhibited continuous inundation throughout the summer, whereas the non-patterned basin was limited to ephemeral ponding following snowmelt (Fig. 6). A connected trough-network in the HCP scenario significantly increased the runoff compared to the LCP-dominated landscape, but only if a realistic, non-homogeneous snow distribution was used (that is, deep snow in troughs). The total runoff from the HCP-dominated basin was similar to the non-patterned domain when the snow was homogeneously distributed. Accordingly, given identical landscape-scale average snow water equivalent, which was observed in the field, not accounting for the heterogeneous snow distribution in HCP tundra can ultimately result in a significant underestimation of runoff. Our model simulations suggest that the observed morphological change, in

© 2016 Macmillan Publishers Limited. All rights reserved

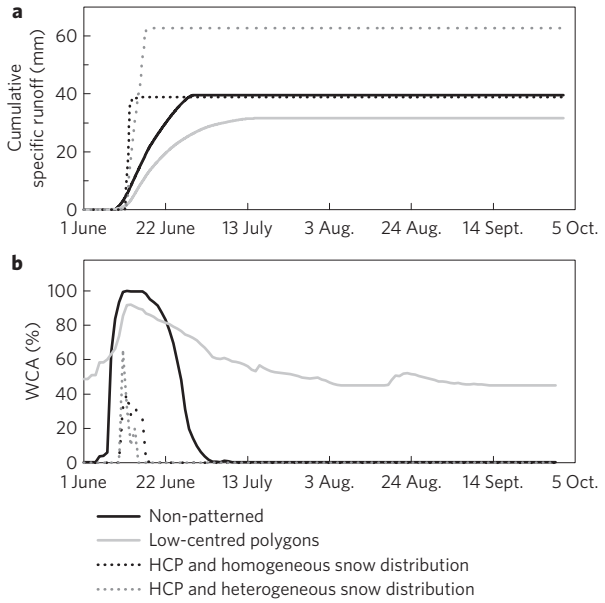

Figure 6 | Model experiments of runoff and inundation using differing polygon types and snow distribution. a,**b**, Simulated runoff (**a**) and water covered area (WCA, **b**) from the four scenarios; a non-patterned ground basin (solid black line), a watershed dominated by LCPs (solid grey line), and HCPs with connected troughs, with deeper snow accumulation in troughs versus mounds (grey dotted line) and a spatially homogeneous end-of-winter snow distribution (black dotted line). End-of-winter snow water equivalent is identical (119 mm) among the four scenarios. LCPs promote lower runoff and extensive inundation, whereas the development of troughs and the subsequent increased spatial variability in snowcover increases runoff and decreases WCA. Note the lack of increased runoff when snow is homogeneously distributed over the HCPs.

particular the development of mounds and laterally connected troughs and its effect on snow distribution, can alone significantly increase runoff and reduce water covered area.

Subsidence linked to press and pulse climate forcing

Landscape-scale ice-wedge degradation is evidently a recent widespread phenomenon at subarctic, Arctic and even High Arctic sites. Our synthesis of field observations, remote sensing and hydrologic modelling documents trough formation across the Arctic continuous permafrost domain with major hydrological implications. The connected trough-network formation and the effect of troughs on snow distribution could potentially intensify the Arctic hydrological cycle alone by significantly increasing runoff despite any changes in snow- or rainfall. Unlike the gradual 'press' long-term warming of permafrost temperatures (Supplementary Fig. 8), which span multiple decades, the ice-wedge degradation appeared as a relatively temporally constrained, sub-decadal 'pulse' phenomenon occurring at landscapes with cold mean annual permafrost temperatures (down to −14 °C, Supplementary Table 1). Accordingly, the process of crossing the local threshold for ice-wedge stability may be favoured by a press occurrence (long-term, gradual increases in air temperatures and/or possibly winter precipitation), but it is probably initiated by pulse atmospheric forcing such as extreme summer warmth and/or winter precipitation (Fig. 2 and Supplementary Fig. 8), as also noted by others in Prudhoe Bay (for example, refs 12,20,28). Increased variability in weather, and in particular summer warmth, may therefore promote ice-wedge degradation to a larger extent than a gradual climate warming alone.

Observed hydrological changes associated with ground subsidence included an increased abundance of trough-ponds and decrease in polygon centre-ponds, leading to increased wetness contrasts across the low-gradient landscape (initial degradation stage with disconnected troughs). The later phase was represented by an overall landscape drying as troughs formed a drainage system (advanced degradation stage with connected troughs), which appear to occur immediately at sites with more slope (for example, Isachsen). Thus, ice-wedge degradation in sloping terrain (∼2% slope) may be more likely to reach the threshold to lateral surface water connectivity, and decades sooner, than in lower-gradient tundra. The onset of the initial stage was abrupt (sub-decadal), although the trough expansion and widening and changes in tundra plant species composition remained active for a decade or more. Here, a combination of atmospheric forcing (that is identical across a landscape) and marked spatiotemporal differences in local feedbacks, which are controlled by factors such as differential snow accumulation, vegetation, sedimentation and hydrology, probably sustained, enhanced, buffered and/or reversed the ground subsidence through the following decades[20]. The documented differential ground subsidence at a few tens of centimetres may be perceived as small locally, but has the potential to significantly impact the regional ecosystem, as ice-rich permafrost may underlie up to two-thirds of the terrestrial Arctic.

Methods

Methods and any associated references are available in the online version of the paper.

Received 27 February 2015; accepted 10 February 2016; published online 14 March 2016

References

1. CAVM Team *Circumpolar Arctic Vegetation Map. (1: 7,500,000 scale), Conservation of Arctic flora and fauna (CAFF) Map No. 1.* (US Fish and Wildlife Service, 2003).
2. Hugelius, G. *et al*. Estimated stocks of circumpolar permafrost carbon with quantified uncertainty ranges and identified data gaps. *Biogeosciences* **11,** 6573–6593 (2014).
3. Schuur, E. A. *et al*. Vulnerability of permafrost carbon to climate change: implications for the global carbon cycle. *BioScience* **58,** 701–714 (2008).
4. Smith, L. C., Sheng, Y., MacDonald, G. & Hinzman, L. Disappearing Arctic lakes. *Science* **308,** 1429–1429 (2005).
5. Jones, B. M. *et al*. Modern thermokarst lake dynamics in the continuous permafrost zone, northern Seward Peninsula, Alaska. *J. Geophys. Res.* **116,** G00M03 (2011).
6. Andresen, C. G. & Lougheed, V. L. Disappearing Arctic tundra ponds: Fine-scale analysis of surface hydrology in drained thaw lake basins over a 65 year period (1948–2013). *J. Geophys. Res. Biogeosci.* **120,** 466–479 (2015).
7. Peterson, B. J. *et al*. Increasing river discharge to the Arctic Ocean. *Science* **298,** 2171–2173 (2002).
8. Rawlins, M. A. *et al*. Analysis of the Arctic system for freshwater cycle intensification: observations and expectations. *J. Clim.* **23,** 5715–5737 (2010).
9. Zhang, X. *et al*. Enhanced poleward moisture transport and amplified northern high-latitude wetting trend. *Nature Clim. Change* **3,** 47–51 (2013).
10. Oelke, C., Zhang, T. & Serreze, M. C. Modeling evidence for recent warming of the Arctic soil thermal regime. *Geophys. Res. Lett.* **31,** L07208 (2004).
11. Zhang, K., Kimball, J. S., Kim, Y. & McDonald, K. C. Changing freeze-thaw seasons in northern high latitudes and associated influences on evapotranspiration. *Hydrol. Process.* **25,** 4142–4151 (2011).
12. Jorgenson, M. T., Shur, Y. L. & Pullman, E. R. Abrupt increase in permafrost degradation in Arctic Alaska. *Geophys. Res. Lett.* **33,** L02503 (2006).
13. Liljedahl, A., Hinzman, L. & Schulla, J. in *Tenth International Conference on Permafrost* (ed. Hinkel, K. M.) 231–236 (The Northern Publisher, 2012).
14. Leffingwell, E. d. K. Ground-ice wedges: the dominant form of ground-ice on the north coast of Alaska. *J. Geol.* **23,** 635–654 (1915).
15. Lachenbruch, A. H. Mechanics of thermal contraction cracks and ice-wedge polygons in permafrost. *Geol. Soc. Am.* **70,** 1–66 (1962).
16. Romanvskii, N. *Formation of Ice Wedges - Polygonal Patterns* [in Russian] (Nauka Publication, 1977).
17. Pollard, W. & French, H. A first approximation of the volume of ground ice, Richards Island, Pleistocene Mackenzie Delta, Northwest Territories, Canada. *Can. Geotech. J.* **17,** 509–516 (1980).
18. Kanevskiy, M. *et al*. Ground ice in the upper permafrost of the Beaufort Sea coast of Alaska. *Cold Reg. Sci. Technol.* **85,** 56–70 (2013).

© 2016 Macmillan Publishers Limited. All rights reserved

19. Ulrich, M., Grosse, G., Strauss, J. & Schirrmeister, L. Quantifying wedge-ice volumes in yedoma and thermokarst basin deposits. *Permafrost Periglac. Process.* **25,** 151–161 (2014).
20. Jorgenson, M. T. *et al*. Role of ground ice dynamics and ecological feedbacks in recent ice wedge degradation and stabilization. *J. Geophys. Res.* **120,** 2280–2297 (2015).
21. Romanovsky, V. E., Smith, S. L. & Christiansen, H. H. Permafrost thermal state in the polar Northern Hemisphere during the International Polar Year 2007–2009: a synthesis. *Permafrost Periglac. Process.* **21,** 106–116 (2010).
22. Couture, N. J. & Pollard, W. H. Modelling geomorphic response to climatic change. *Climatic Change* **85,** 407–431 (2007).
23. Shiklomanov, N. I., Streletskiy, D. A., Little, J. D. & Nelson, F. E. Isotropic thaw subsidence in undisturbed permafrost landscapes. *Geophys. Res. Lett.* **40,** 6356–6361 (2013).
24. Jones, B. M. *et al*. Quantifying landscape change in an Arctic coastal lowland using repeat airborne LiDAR. *Environ. Res. Lett.* **8,** 045025 (2013).
25. Günther, F. *et al*. Observing Muostakh disappear: permafrost thaw subsidence and erosion of a ground-ice-rich island in response to Arctic summer warming and sea ice reduction. *Cryosphere* **9,** 151–178 (2015).
26. Jorgenson, J. C., Raynolds, M. K., Reynolds, J. H. & Benson, A.-M. Twenty-five year record of changes in plant cover on tundra of northeastern Alaska. *Arct. Antarct. Alp. Res.* **47,** 785–806 (2015).
27. Necsoiu, M., Dinwiddie, C. L., Walter, G. R., Larsen, A. & Stothoff, S. A. Multi-temporal image analysis of historical aerial photographs and recent satell te imagery reveals evolution of water body surface area and polygonal terrain morphology in Kobuk Valley National Park, Alaska. *Environ. Res. Lett.* **8,** 025007 (2013).
28. Raynolds, M. K. *et al*. Cumulative geoecological effects of 62 years of infrastructure and climate change in ice-rich permafrost landscapes, Prudhoe Bay Oilfield, Alaska. *Glob. Change Biol.* **20,** 1211–1224 (2014).
29. Steedman, A. E. *The Ecology and Dynamics of Ice Wedge Degradation in High-Centre Polygonal Terrain in the Uplands of The Mackenzie Delta Region, Northwest Territories, Canada* MS thesis, Univ. Victoria (2014).
30. Engstrom, R., Hope, A., Kwon, H., Stow, D. & Zamolodchikov, D. Spatial distribution of near surface soil moisture and its relationship to microtopography in the Alaskan Arctic Coastal Plain. *Nord. Hydrol.* **36,** 219–234 (2005).
31. Webber, P. J. *Vegetation and Production Ecology of an Alaskan Arctic Tundra* 37–112 (Springer, 1978).
32. Webber, P. J. in *An Arctic ecosystem: The Coastal Tundra at Barrow, Alaska* (ed. Brown, J.) 30–56 (Downden, Hutchinson & Ross, 1980).
33. Sommerkorn, M. Micro-topographic patterns unravel controls of soil water and temperature on soil respiration in three Siberian tundra systems. *Soil Biol. Biochem.* **40,** 1792–1802 (2008).
34. Olivas, P. C. *et al*. Effects of fine-scale topography on CO_2 flux components of Alaskan Coastal Plain tundra: response to contrasting growing seasons. *Arct. Antarct. Alp. Res.* **43,** 256–266 (2011).
35. Lara, M. J. *et al*. Polygonal tundra geomorphological change in response to warming alters future CO_2 and CH_4 flux on the Barrow Peninsula. *Glob. Change Biol.* **21,** 1634–1651 (2015).
36. Boike, J., Wille, C. & Abnizova, A. Climatology and summer energy and water balance of polygonal tundra in the Lena River Delta, Siberia. *J. Geophys. Res.* **113,** G03025 (2008).
37. Cresto-Aleina, F. *et al*. A stochastic model for the polygonal tundra based on Poisson-Voronoi diagrams. *Earth Syst. Dynam.* **4,** 187–198 (2013).
38. Helbig, M. *et al*. Spatial and seasonal variability of polygonal tundra water balance: Lena River Delta, northern Siberia (Russia). *Hydrogeol. J.* **21,** 133–147 (2013).
39. Woo, M. K. & Guan, X. J. Hydrological connectivity and seasonal storage change of tundra ponds in a polar oasis environment, Canadian High Arctic. *Permafrost Periglac. Process* **17,** 309–323 (2006).
40. Matveyeva, N. V. & Zanokha, L. L. *Biodiversity of Ecosystems of the Far North: Inventory, Monitoring and Protection* 96–106 (Transactions of All-Russia Scientific Conference, 2013).
41. Frost, G. V. & Epstein, H. E. Tall shrub and tree expansion in Siberian tundra ecotones since the 1960s. *Glob. Change Biol.* **20,** 1264–1277 (2014).
42. Brown, J., Ferrians, O. J. J., Heginbottom, J. & Melnikov, E. *Circum-Arctic Map of Permafrost and Ground-Ice Conditions* Version 2 [Permafrost] (National Snow and Ice Data Center, 2002); http://nsidc.org/data/GGD318

Acknowledgements

Financial assistance was provided by the Next-Generation Ecosystem Experiments (NGEE Arctic) project, which is supported by the Office of Biological and Environmental Research in the Department of Energy Office of Science (DE-AC02-05CH11231), National Science Foundation (OIA-1208927, DPP-1304271, PLR-1204263), Arctic Landscape Conservation Cooperative (ALCC2014-02), the Japan Society for the Promotion of Science (26242026), European Research Council (ERC-338335), Carbon in Arctic Reservoirs Vulnerability Experiment (CARVE) of the National Aeronautics and Space Administration and via the PAGE21 project sponsored by the European Commission (FP7-ENV-2011, no. 282700). Recent high-resolution satellite imagery was provided by the Polar Geospatial Center, University of Minnesota. A. Chamberlain, A. Kholodov and R. Busey provided field and/or data processing support. M. Rohr assisted in designing the schematic figure. C. Tweedie, University of Texas El Paso provided the LiDAR DEM. R. Thoman at the National Ocean and Atmospheric Administration, Fairbanks, provided historical weather observations near Prudhoe Bay. The Arctic Region Supercomputing Center, University of Alaska Fairbanks, offered computational support. This work also used the Extreme Science and Engineering Discovery Environment (XSEDE), which is supported by National Science Foundation (ACI-1053575).

Author contributions

A.K.L. designed the study and wrote the first draft. A.N.F., J.B., G.V.F., G.G., J.C.J., M.N., N M., M.K.R., V.E.R., K.D.T. and D.A.W. provided imagery, photos, site descriptions and meteorology. M.N. performed change-detection image analyses. A.N.F., Y.I., V.E.R. and H.Y. provided permafrost temperatures. A.K.L., J.S. and R.P.D. performed the model experiments. L.D.H. provided elevation and soil moisture measurements and D.Z. the quality-controlled eddy covariance measurements. A.K.L. and C.J.W. designed and executed the water level and snow measurements. All authors contributed to data interpretation and writing of the manuscript.

Additional information

Supplementary information is available in the online version of the paper. Reprints and permissions information is available online at www.nature.com/reprints. Correspondence and requests for materials should be addressed to A.K.L.

Competing financial interests

The authors declare no competing financial interests.

© 2016 Macmillan Publishers Limited. All rights reserved

Methods

Data. Mean daily air temperatures and total daily precip tation were obtained from the nearest long-term meteorological station via National Ocean and Atmospheric Administration (NOAA) and RosHydroMet archives (https://gis.ncdc.noaa.gov, Supplementary Table 2). Long-term permafrost temperatures (Supplementary Table 1) were obtained from permafrost observatories that are included in the Global Terrestrial Network for Permafrost[43] (https://www.aoncadis.org/dataset/network_of_permafrost_observatories_in_north_america_and_russia.html). Field observations for permafrost temperatures used in model validation were obtained from the '*Barrow2*' site at the Geophysical Institute Permafrost Laboratory data archive (http://permafrost.gi.alaska.edu). Water levels and snow surveys (Figs 4 and 5) are available at the Next-Generation Ecosystem Experiment, NGEE–Arctic[44,45]. Measured evapotranspiration that were used in model validation is available at the AmeriFlux archive as site '*US-Bes*' (http://ameriflux.ornl.gov). Active layer soil temperatures, runoff and snow ablation used in model validation are available as Excel-readable files separate to the Supplementary Information. Locations of sites used in model validation are presented in Supplementary Fig. 9. High-resolution images of Samoylov were obtained from ref. 46.

Analyses. Methods for image change-detection analyses, orthorectification and co-registration were based on the approaches of Necsoiu and others[27]. All data sets have 1-m or better ground resolution (Supplementary Table 3), with the exception of two data sets (the 1960's imagery of Corona/Chukochy and Corona/Samoylov), resulting in an overall error in registration of <1 m, although at some sites these errors were much lower (for example, $\sim 0.02 \pm 0.74$ m at Kobuk). For example, in Kolyma the imagery was co-registered with reference to individual larch trees. The selected thresholds for the automatic change detection were designed to identify extreme changes between image pairs. The threshold values were defined on the basis of image interpretation, professional judgement and expertise of the local conditions. All ice-wedge degradation sites represent our field study locations, where on-site visits (for other studies than ice-wedge degradation) confirmed the differential ground subsidence. We analysed imagery from mid- to late summer and early fall to avoid the typical snowmelt-driven early-summer inundation period. A compilation of summer cumulative precipitation, including long-term averages, presents an antecedent precipitation regime for respective image/photo (Supplementary Fig. 10). All observed sites/dates align near or below the cumulative long-term average, except Barrow, which experienced a large precip tation event just prior the 2010 image. However, the trough development since 1948 in Barrow is also shown in the 2007 image (Supplementary Fig. 7), which was a record low precipitation summer[47]. Therefore, unusual summer precip tation and resulting high surface water are not responsible for the new ponds that were observed.

Winter precipitation was defined as the total precipitation during months with average monthly temperatures below 0 °C. Daily precipitation included recordings of trace amounts, by the add tion of 0.1 mm (ref. 48). Cumulative summer precip tation represented the period 1 June–30 September. Incomplete recordings at the Isachsen weather station (GHCND CA002402604) during several recent years resulted in the use of the more complete data set at Eureka. A comparison between the Eureka and the two Isachsen weather stations is given in Supplementary Fig. 11. All sites show a warming trend in MAAT and SWI.

The sensor for air temperature measurements at the Isachsen ice-wedge degradation site was a Campbell L-107 thermistor installed into the Campbell soil radiation shield at 2 m above the ground surface (referred to as the 'UAF' site). Ground temperature was measured using calibrated MRC thermistor string. The accuracy of measurements was 0.1 °C. Water levels near Barrow were measured using a non-vented Cera-Diver DI701 (Schlumberger Water Services, Pressure: Range 10 m, accuracy ±0.5 cm, resolution 0.2 cm) in 2013 and 2014 and Capacitance Water Level Recorders (Odyssey Dataflow Systems, Probe length 1 m, resolution 0.8 mm) in 2012. Loggers recorded at 15 min intervals. The Cera-Divers were manually lowered on a sub-monthly basis (June and July), as the active layer thaw progressed, and removed in September. Manual measurements of water level were conducted to establish a reference for calibration. Loggers were hung using a nylon string inside the wells, which were installed in spring 2012 using a 5-cm-diameter SiPRE corer. The wells were represented by ~32-mm-diameter white PVC pipe (Supplementary Fig. 9b) about ~160 cm long with ~6-mm-diameter holes drilled about 1–2.5 cm apart in three transects along the side walls. The wells were anchored about 30 cm into the permafrost by three bolts protruding from the side of the PVC pipe by approximately 0.5–1 cm. Manual water levels were measured as the distance from a mark near the top of the pipe to the water surface. Data from the non-vented pressure transducers were adjusted for atmospheric pressure following the standard procedures in the Schlumberger processing software. The capacitance probes were cleaned regularly. Water level measurements for model validation were those described and presented by others[49]. Several hundred snow depth measurements were made on 4–5 May at ~0.3 m intervals, which at the LCP and HCP site covered approximately 50 × 50 and 30 × 30 m domains, respectively, along parallel transects located ~5 and 3 m apart, respectively. The depth measurements were made using an automated snow depth probe (SnowHydro).

We applied the physically based hydrological model Water balance Simulation Model, WaSiM, which includes mass and heat transfer, to evaluate the role of ice-wedge polygon type (that is, the impact of ice-wedge degradation) and snow distribution on watershed-scale runoff and inundation. It should be noted that the simulations did not dynamically represent ground subsidence, but rather presented three fixed DEM scenarios (non-patterned ground, low- and high-centred polygons)—each with unique topographic features aimed at representing the observed key degradation stages or polygon types. Nor were ice wedges included in the soil parametrization. For a more detailed model description, parameterization and validation, see the Supplementary Methods.

The schematic model domain for the experiments presented in Fig. 6 was derived from a LiDAR digital elevation model representing a 90 × 90 m area in 0.25-m resolution of polygonal tundra in Barrow, Alaska (Supplementary Figs 9 and 12). The original 0.25 × 0.25 m-pixel LiDAR elevation map was first averaged into 20 × 20 m pixels to create a gently sloping 'base-surface'. Second, the base-surface was returned to a 0.25-m resolution, resulting in a smoothed elevation map that by itself represented the non-patterned scenario and the foundation for other model experiments (high- or low-centred polygon dominated basins). Third, the polygon features of rims or troughs were manually outlined by following the observed (LiDAR) patterns. The maximum height of the rims or mounds were constrained to 20 and 40 cm, respectively. The model experiments were forced using measured hourly meteorology from Barrow (June 1999–May 2000) and end-of-winter snow depth measurements from the Barrow Circumpolar Active Layer Monitoring grid. Average watershed SWE before onset of snowmelt was identical between the scenarios (119 mm), although the sub-basin distribution of snow varied between the scenarios, where the snow was distributed to result in a snow surface that was identical to the non-patterned ground surface in the LCP and HCP scenarios (that is, deeper snow in depressions); and homogeneously in the non-patterned and also in a second simulation of the HCP scenario. Soil property profiles were identical throughout the schematic watershed experiment with a 10-cm-thick organic mat and underlying silt. Parameter values used in simulations are presented in Supplementary Tables 4–6. The model was run into a semi-equilibrium hydrologic state, which was achieved after two to three model years. Similar model experiments, which were forced by an 11-yr period of Barrow forcing data (1999–2009) and that excluded seasonal freeze and thaw, show the influence of ice-wedge polygon type on individual water balance components to be consistent from year to year[13].

Code availability. The compiled code of WaSiM is accessible for anyone to download online (http://www.wasim.ch) and the key equations that underlay the two not previously published modules are presented in the Supplementary Methods. A detailed description of all key equations can be found in the user manual, which is available at the WaSiM website.

References

43. Burgess, M., Smith, S., Brown, J., Romanovsky, V. & Hinkel, K. *The Global Terrestrial Network for Permafrost (GTNet-P): permafrost monitoring contributing to global climate observations* Current Research 2000 E14 (Geological Survey of Canada, 2000).
44. Liljedahl, A. K. & Wilson, C. J. *Water Levels, Barrow, Alaska, NGEE Areas A, B, C and D for 2012, 2013, 2014* Final Version, 20150324 (NGEE Arctic, 2016); http://dx.doi.org/10.5440/1183767
45. Liljedahl, A. K. & Wilson, C. J. *Snow, End-of-Winter, Intensive Site 1, Area A, B, C and D, 2012 to 2014, Barrow, Alaska* (NGEE Arctic, 2016); http://dx.doi.org/10.5440/1236472
46. Muster, S., Langer, M., Heim, B., Westermann, S. & Boike, J. Subpixel heterogeneity of ice-wedge polygonal tundra: a multi-scale analysis of land cover and evapotranspiration in the Lena River Delta, Siberia. *Tellus B* **64,** 17301 (2012).
47. Liljedahl, A. K. *et al*. Nonlinear controls on evapotranspiration in Arctic coastal wetlands. *Biogeosciences* **8,** 3375–3389 (2011).
48. Yang, D., Goodison, B. E., Ishida, S. & Benson, C. S. Adjustment of daily precipitation data at 10 climate stations in Alaska: application of World Meteorological Organization intercomparison results. *Wat. Resour. Res.* **34,** 241–256 (1998).
49. Goswami, S., Gamon, J. A. & Tweedie, C. E. Surface hydrology of an Arctic ecosystem: multiscale analysis of a flooding and draining experiment using spectral reflectance. *J. Geophys. Res.* **116,** G00107 (2011).

© 2016 Macmillan Publishers Limited. All rights reserved